Cosmological hydrogen recombination: populations of the high level sub-states

J. Chluba[1⋆], J. A. Rubiño-Martín[2]† and R.A. Sunyaev[1,3]
[1] *Max-Planck Institut für Astrophysik, Karl-Schwarzschild-Str. 1, D-85740 Garching, Germany*
[2] *Instituto de Astrofísica de Canarias, C/Vía Láctea s/n, E-38200 Tenerife, Spain*
[3] *Space Research Institute (IKI), Russian Academy of Sciences, Profsoyuznaya 84/32 Moscow, Russia*

Received **insert**; Accepted **insert**

ABSTRACT
We present results for the spectral distortions of the Cosmic Microwave Background (CMB) arising due to bound-bound transitions during the epoch of cosmological hydrogen recombination at frequencies down to $\nu \sim 100\,\mathrm{MHz}$. We extend our previous treatment of the recombination problem (Rubiño-Martín et al. 2006) now including the main collisional processes and following the evolution of all the hydrogen angular momentum sub-states for up to 100 shells. We show that, due to the low baryon density of the Universe, even within the highest considered shell full statistical equilibrium (SE) is not reached and that at low frequencies the recombination spectrum is significantly different when assuming full SE for $n > 2$. We also directly compare our results for the ionization history to the output of the RECFAST code, showing that especially at low redshifts rather big differences arise. In the vicinity of the Thomson visibility function the electron fraction differs by roughly -0.6% which affects the temperature and polarization power spectra by $\lesssim 1\%$. Furthermore we shortly discuss the influence of free-free absorption and line broadening due to electron scattering on the bound-bound recombination spectrum and the generation of CMB angular fluctuations due to scattering of photons within the high shells.

Key words: atomic processes – cosmic microwave background – spectral distortions – cosmology: theory – early Universe

1 INTRODUCTION

The study of the Cosmic Microwave Background (CMB) provides one of the most powerful tools to test cosmological models and to determine the parameters describing the Universe. Nowadays, most of the CMB experiments are focused on the study of the temperature and polarization angular fluctuations, which have been measured recently with very high precision by the WMAP satellite (Page et al. 2006; Hinshaw et al. 2006), permitting to achieve accuracies in the determination of some of the key cosmological parameters on the level of a few percent.

The CMB photons which are detected today were essentially last scattered towards us during the epoch of cosmological recombination, where the temperature of the Universe had become sufficiently low to permit the formation of neutral atoms (Zeldovich et al. 1968; Peebles 1968). During the process of cosmological recombination of the hydrogen and helium atoms there was a net generation of photons, which introduces distortions to the CMB blackbody spectrum. Except for the far Wien tail of the CMB, these distortions are expected to be very small: the distortions due to bound-bound transitions reach the level of $\Delta I/I \sim 10^{-7}$ at frequency $\nu \sim 1\,\mathrm{GHz}$ and are smaller than $\Delta I/I \sim 10^{-8}$ in the range $10\,\mathrm{GHz} \leqslant \nu \leqslant 500\,\mathrm{GHz}$ (e.g. see Rubiño-Martín et al. 2006, RMCS06 hereafter). This is mainly due to the extremely large entropy of the Universe (there are $\sim 1.6 \times 10^9$ photons per baryon), since in the presence of undistorted blackbody radiation there cannot be much more than one photon per transition (Liubarskii & Sunyaev 1983). The free-bound emission increases the spectral distortions by additional $\sim 30-90\%$ and a total ~ 5 photons per hydrogen atom are released due to hydrogen recombination in the undistorted ambient blackbody photon field of the CMB (Chluba & Sunyaev 2006a). However, a measurement of these tiny deviations from a pure blackbody would provide another independent way to determine some of the key cosmological parameters, such as the baryon density or the total matter content. In addition they in principle are a *byproduct* of the accurate treatment of the recombination history and in particular the time depen-

⋆ E-mail: jchluba@mpa-garching.mpg.de
† E-mail: jose.alberto.rubino@iac.es

dence of the free electron fraction in the Universe, which today is so important for the theoretical prediction of the CMB temperature and polarization power spectra.

The numerical solution of the hydrogen recombination history and the associated spectral distortions of the CMB requires the integration of a stiff system of coupled ordinary differential equations, describing the evolution of the populations of the different hydrogen levels, with extremely high accuracy, simply because the amplitude of the distortions is so small. Several authors have computed the distortions due to bound-bound transitions for a multi-level hydrogen atom with different assumptions and simplifications (Dubrovich 1975; Beigman & Sunyaev 1978; Rybicki & dell'Antonio 1993; Dubrovich & Stolyarov 1995; Dubrovich & Shakhvorostova 2004; Kholupenko et al. 2005; Wong et al. 2006, RMCS06). Among these the most important simplification is to assume *full statistical equilibrium*[1] (SE) within a given shell for $n > 2$ (for a more detailed comparison of the different approached see RMCS06 and references therein). With this assumption the recombination problem becomes significantly simpler, since for each additional shell only one more equation has to be treated, and Kholupenko et al. (2005) already presented results for the hydrogen recombination spectrum due bound-bound transitions in the frequency range $1\,\mathrm{GHz} \leqslant \nu \leqslant 1000\,\mathrm{GHz}$ including up to 160 shells within this approximation.

In our previous work (RMCS06) the spectral distortions of the CMB spectrum arising due to bound-bound transitions and the 2s two-photon decay during the epoch of cosmological hydrogen recombination were obtained in the frequency range $1\,\mathrm{GHz} \leqslant \nu \leqslant 3500\,\mathrm{GHz}$. There the complete set of ordinary differential equations was solved for the cosmological hydrogen recombination problem including up to 30 shells, with *all* the energetically degenerate angular momentum sub-levels treated separately. It was shown that assuming SE for shells $n > 2$ leads to significant differences in the cosmological hydrogen recombination spectrum for the Balmer, Paschen and Brackett series. Furthermore, it was argued that collisions probably can only become important for shells well above $n \sim 25 - 30$, so that assuming SE for the lower shells is not justified, but a detailed examination of this problem has not been performed until now.

In this paper, we present detailed results for the hydrogen recombination spectrum due to bound-bound transition at low frequencies down to $\nu \sim 100\,\mathrm{MHz}$ (see Fig. 2). To this end, we have solved the complete set of equations for a multi-level hydrogen atom with 100 shells, i.e. we are following the populations of 5050 separate hydrogen states. Furthermore, we include the main collisional processes into our calculations (for more details see Sect. 2.1) and discuss deviations from full SE within the high shells. We also examine the influence of the free-free process (Sect. 4.1) at low frequencies, the line broadening due to electron scattering (Sect. 4.2) and the generation of CMB angular fluctuations by scattering of photons within the high shells (Sect. 4.3). For the treatment of the multi-level hydrogen atom we basically follow the same procedure as described in RMCS06, with some modification which are explained in Sect. 2.

Several authors have worked on percent level corrections to the ionization history arising from different previously neglected physical processes (Dubrovich & Grachev 2005; Chluba & Sunyaev 2006b; Kholupenko & Ivanchik 2006; Novosyadlyj 2006). It was pointed out that these corrections lead to differences in the theoretical predictions for the CMB temperature and polarization power spectra on a similar level and therefore should be taken into account when analyzing future high precision data. Recently, Lewis et al. (2006) have made some first steps towards quantifying the possible impact of percent level correction to the ionization history on the estimation of cosmological parameters, again showing that in the era of precision cosmology more efforts should be made to improve the calculation of the recombination history.

In RMCS06 it was also pointed out that there are corrections to the ionization history on the level of percent arising due to the detailed treatment of the angular momentum sub-states of the hydrogen atom. With computations including up to 100 shells, one reaches the point to directly compare the obtained ionization history with the output of the RECFAST code, which was developed to represents the computations based on a 300-level hydrogen atom (Seager et al. 1999), but under the assumption of SE for $n > 2$. We shall discuss our results for the obtained electron recombination history as compared to the RECFAST output in Sect. 3.3 and show that especially at low redshifts rather big differences arise. However, still more work has to be done to reach percent level accuracy for the ionization history.

For all the computation presented in this work the following values of the cosmological parameters were adopted: $\Omega_\mathrm{b} = 0.0444$, $\Omega_\mathrm{tot} = 1$, $\Omega_\mathrm{m} = 0.2678$, $\Omega_\Lambda = 0.7322$, $Y_\mathrm{p} = 0.24$, $h = 0.71$ and $T_0 = 2.725\,\mathrm{K}$.

2 COMPUTATIONAL ISSUES

In general we use the same approach and definitions as in RMCS06. However, in order to solve the full problem for $n_\mathrm{max} \geqslant 30$ we had to improve the computational treatment significantly. Therefore we modified one of our previous codes to include the most important collisional processes and made some more simplifying assumptions, which we shall briefly discuss in this Section.

2.1 Inclusion of collisions

It was pointed out in RMCS06 that the assumption of SE is equivalent to *instantaneous redistribution* of the electrons within a given shell. Especially for hydrogen levels (n, l) with large angular momentum quantum number $(0 \ll l \leqslant n-1)$ this assumption changes the populations strongly, because for high shells due to the l-dependence of the recombination Gaunt-factor direct recombinations to these levels become very unlikely. This point is illustrated in Fig. 1, where we show the l-dependence of the recombination coefficients α_{nl} for different shells[2]. One can clearly see, that for large n most

[1] i.e. the population of a given level (n, l) is determined by $N_{nl} = (2l+1)N_n/n^2$, where N_n is the total population of the shell with principle quantum number n.

[2] Here α_{nl} is defined such that $N_\mathrm{e}\,N_\mathrm{p}\,\alpha_{nl}$ is the change of the population of level (n, l) due to direct recombinations per sec-

of the electrons recombine to states with $l/l_{\rm max} \sim 0.1-0.2$. Therefore in the full problem electrons mainly reach levels with large n and l connecting to other levels via radiative and collisional transitions, where the former are very inefficient, since they proceeds via many intermediate states, and latter, due to the large entropy of the Universe, are rather slow. However, due to the $\Delta l = \pm 1$ restriction for radiative dipole transitions, levels with large n and l quantum numbers will depopulate rather slowly via low frequency transitions which leads to a delicate interplay between all the rates connecting to the neighboring levels.

In Fig. 1 for $n = 100$ we also give the recombination coefficient within the Kramers' approximation. Here the dependence on the recombination Gaunt-factor is neglected such that the l-dependence of the recombination coefficient only enters due to the fact that *one single* electron can find $(2l + 1)$ sub-levels to be captured to. Hence, within the Kramers' approximation electrons preferentially recombine to states with large l. On the other hand, it is clear that within the Kramers' approximation the photoionization process is also more effective for high l-states, which implies that after any disturbance for these levels full equilibrium with the continuum is reached on a much shorter time-scale. Since here we are looking for *tiny* deviations from full equilibrium therefore it is important to include the Gaunt-factors into the computations and to account for collisions which help changing the populations of high l-states.

From Fig. 1 one can also see that explicitly neglecting *induced recombinations*, but including the Gaunt-factor, significantly alters the l-dependence of recombination coefficient for large n. In addition the total recombination rates for high shells strongly decreases for this case. Below, we now outline which collisional processes were accounted for in the present paper.

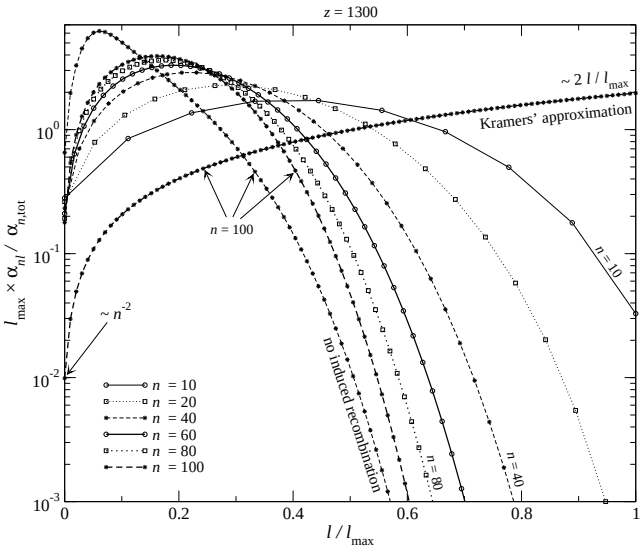

Figure 1. l-dependence of the recombination coefficient, α_{nl}, at $z = 1300$ for different shells. The curves have been re-scaled by the *total* recombination coefficient, $\alpha_{n,\rm tot} = \sum_l \alpha_{nl}$, and multiplied by $l_{\rm max} = n - 1$ such that the 'integral' over $\xi = l/l_{\rm max}$ becomes unity. Also the results obtained within the Kramers' approximation, i.e. $\alpha^{\rm K}_{nl} = {\rm const} \times [2l+1]$, and without the inclusion of stimulated recombination for $n = 100$ are presented.

2.1.1 l-changing collisions

One of the most important differences with respect to our previous computations (RMCS06) is that we now also include collisions of the form $(n, l) \rightarrow (n, l \pm 1)$. These are important in order to *restore* and *maintain* full statistical equilibrium (SE) within a given shell and from simple estimates (Pengelly & Seaton 1964) for the conditions like in our Universe one expects that within the redshift range $500 \leqslant z \leqslant 2500$ these start contributing for shells with principal quantum numbers $n \gtrsim 25 - 30$. The corresponding coupling term for the population N_{nl} of level (n, l) to the populations $N_{nl'}$ of level (n, l') with $l' = l \pm 1$ due to the collision with a particle of species i is then given by

$$\left.\frac{\partial N_{nl}}{\partial t}\right|_{\rm i}^{l-{\rm coll}} = \left[\frac{(2l+1)}{(2l'+1)}\frac{N_{nl'}}{N_{nl}} - 1\right] N_{nl} C_{nl\rightarrow nl'}\,, \quad (1)$$

We calculate the collision rates $C_{nl\rightarrow nl'}$ according to Brocklehurst (1971).

Since the energy of the bound electron is not changing, in contrast to n-changing collisions the mass of the projectile is more important than its velocity. Therefore the l-changing collision rates due to proton impact are usually larger than for electron impact, but we included both into our calculations. Also collisions with He II ions were accounted for, but due to their low number density and the history of He II recombination they only lead to a $\lesssim 10\%$ contribution to the total collision rate at redshifts $z \gtrsim 1500$. Since the lines due to hydrogen recombination typically appear at redshifts $z \lesssim 1500$, He II collisions basically do not affect the final results for the bound-bound spectral distortion.

In order to speed up our computation we tabulate the l-changing collision rates before starting to solve the system of coupled ordinary differential equations, assuming that a sufficient approximation to the electron temperature $T_{\rm e}$ and electron, proton and He II number densities is given by the results from the RECFAST code (Seager et al. 1999). Since in general the approximations for the collisional rates are only accurate on the level of $\sim 10\% - 50\%$ this should be a reasonable approach.

One should mention that in principle the $\Delta l = \pm 1$ restriction does not apply for l-changing collisions and coupling terms with $|\Delta l| > 1$ could be important, but smaller due to the decrease of the cross section with growing Δl. These should help to bring the populations for a given shell faster into full SE than in the calculations presented here. However, we neglected those terms for the moment.

2.1.2 n-changing collisions

Energy or n-changing collisions of the type $(n, l) \rightarrow (n', l\pm1)$ with $n \neq n'$ are usually less important than l-changing collisions (e.g. see comments in Sect. 3.2.4 of Hummer & Storey 1987). But since here we are discussing highly excited electron states in the hydrogen atom we decided to include collisional excitation and de-excitation as well and check their influence on the recombination spectrum. However, we are

ond, where $N_{\rm e}$ and $N_{\rm p}$ are the free electron and proton number densities, respectively.

not including collisional ionization or three-body recombination, since the relevance of these processes is expected to be even smaller.

As mentioned above, for energy-changing collisions the velocity of the projectile is important and hence the n-changing collision rate is dominated by the contribution from electron impact. We shall only consider collisional excitation and de-excitation by electrons, but neglect the corresponding processes induced by protons, He II ions or neutral hydrogen atoms.

For collisional processes a vast amount of literature can be found, all based on different assumptions and approximations. Here we decided to use the simple approximations as given by van Regemorter (1962). These likely are only accurate to within a factor of $\sim 2-10$ probably even up to ~ 100, but they are very fast for numerical evaluations and widely used in computations of stellar atmospheres. The corresponding coupling term for the population N_{nl} of level (n,l) to the populations $N_{n'l'}$ of level (n',l') due to the collision with an electron is then given by

$$\left.\frac{\partial N_{nl}}{\partial t}\right|_{\rm e}^{n-{\rm coll}} = \left[\frac{(2l+1)}{(2l'+1)}\frac{N_{n'l'}}{N_{nl}}\,e^{-\frac{\Delta E}{kT_{\rm e}}}-1\right]N_{nl}C_{nl\rightarrow n'l'}\,, \tag{2}$$

where ΔE is the energy difference of the considered levels. We calculate the collisional de-excitation rate $C_{nl\rightarrow n'l'}$ for electron impact according to formula (18) in the work of van Regemorter (1962). Only radiatively allowed transitions are taken into account here. Note that since collisions are controlled by electrons, the electron temperature appears in the exponential factor of (2).

2.2 Additional comments

The computations of the photoionization and photorecombination rates involve 1-dimensional integrals over the ambient photon field. These have to be evaluated many times in order to solve the problem. Since we assume that the ambient photon field is a pure blackbody, the only coupling to the current solution arises due to the electron temperature. For up to 50 shells we have checked that instead of evaluating both the photoionization and photorecombination rates at every time it is sufficient to use the photorecombination rate *only* and apply the detailed balance relation. Since this approximation is possible one can again tabulate the photorecombination rates using the results for the electron temperature from the RECFAST code and then interpolate. In this way one speeds up the computation by a large factor. For 50 shells we have compared the results obtained with and without this simplification and found practically no difference in the recombination spectrum. This is because at $z\sim 1100-1400$, i.e. where the lines form, the difference in the electron and photon temperature is very small ($\Delta T/T\sim 10^{-6}-10^{-5}$). One should also mention that we evaluated the photoionization cross section and radiative rates as described in Storey & Hummer (1991), since for $n\gtrsim 50$ the expressions given by Karzas & Latter (1961) were numerically unstable.

In addition it is important to use both relative and absolute error control. The solvers D02NBF and D02NGF from the NAG-Library[3] provide this possibility. We usually requested $\epsilon\sim 10^{-8}$ relative and $\epsilon\sim 10^{-22}-10^{-23}$ or less absolute error. Furthermore at low redshifts we had to limit the maximal step-size to $h\sim 0.1-0.5$. We also ran computations with increased accuracies but found no significant differences. With these settings one computation of the recombination spectrum for $n_{\rm max}=n_{\rm split}=100$ took about 6 days on a $\sim 3\,$GHz single processor machine.

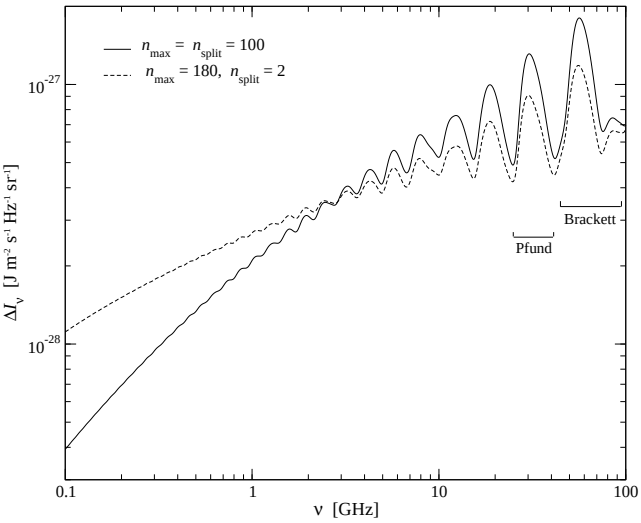

Figure 2. The hydrogen bound-bound emission spectrum at low frequencies. In the full computation ($n_{\rm max}=n_{\rm split}=100$) the evolution of all the angular momentum sub-states was taken into account separately including collisions. For comparison we also show the results obtained with $n_{\rm max}=180$ and $n_{\rm split}=2$. The contribution due to the 2s two-photon decay is negligible within the considered range of frequencies and was therefore omitted.

3 RESULTS AND DISCUSSION

3.1 The hydrogen bound-bound emission spectrum at low frequencies

In Figure 2 we present the hydrogen recombination spectrum for bound-bound transitions at low frequencies. In our full computation ($n_{\rm max}=n_{\rm split}=100$) the evolution of *all* the angular momentum sub-states was taken into account separately and l- and n-changing collisions were included. In this calculation the evolution of 5050 separate hydrogen states in the redshift range of $200\leqslant z\leqslant 2100$ was followed. Due to computational limitations this was the largest calculation we were able to perform within reasonable time. For comparison we also show the results obtained with $n_{\rm max}=180$ under the simplifying assumption of SE for shell with $n>2$, i.e. $n_{\rm split}=2$.

For the full calculation ($n_{\rm max}=100$ and $n_{\rm split}=100$) within the frequency range $1\,{\rm GHz}\leqslant\nu\leqslant 100\,{\rm GHz}$ one can clearly see the low contrast features, which were also discussed in RMCS06. As expected, here due to the inclusion of more shells the level of the distortions is higher than in RMCS06, but at $\nu\lesssim 2\,$GHz they do not reach the level obtained in the case $n_{\rm max}=180$ and $n_{\rm split}=2$. At 1 GHz these

[3] see http://www.nag.co.uk/

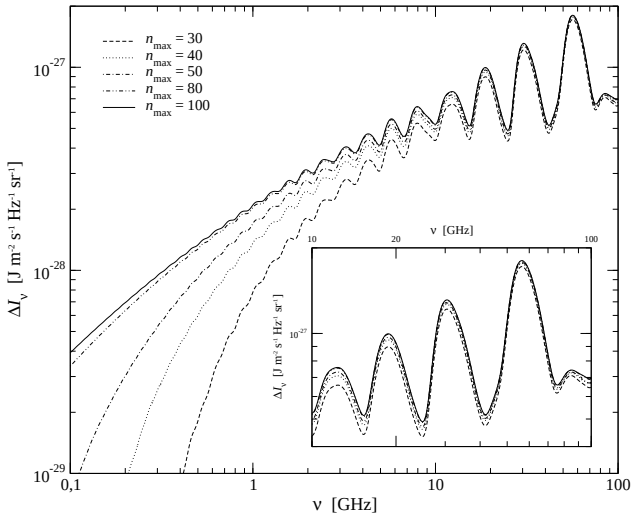

Figure 3. The hydrogen bound-bound emission spectrum at low frequencies for different $n_{\rm max}$ and $n_{\rm split} = n_{\rm max}$. Also l- and n-changing collisions were included.

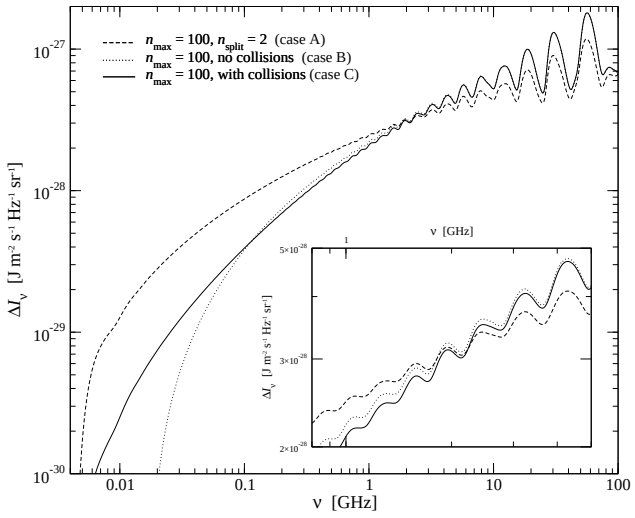

Figure 4. Effect of collisions on the hydrogen bound-bound emission spectrum at low frequencies. Free-free absorption was not taken into account.

two solutions differ by a factor of ~ 1.4 (see Section 3.1.2 for more discussion). Below $\sim 1\,$GHz the spectral distortions become practically featureless. In the frequency range $1\,{\rm GHz} \lesssim \nu \lesssim 10\,{\rm GHz}$ the slope of the spectrum is $\beta \sim 0.46$ and therefore slightly steeper than the one obtained in the calculations of Kholupenko et al. (2005) and our $n_{\rm max} = 180$ and $n_{\rm split} = 2$ case, i.e. $\beta \sim 0.35$.

3.1.1 Convergence with $n_{\rm max}$

To estimate the convergence of the results for the hydrogen recombination spectrum at low frequencies we computed the distortions for different $n_{\rm max}$ (see Fig. 3). At $\nu \sim 1\,$GHz for $n_{\rm max} = 100$ the spectral distortion is a factor of ~ 2.6 larger than for $n_{\rm max} = 30$. One can see that at $\nu \geqslant 1\,$GHz the distortion is practically not changing anymore when including more than ~ 80 shells. Within our assumption the results should be converged on a level of $\sim 10-20\%$ at frequencies $0.1\,{\rm GHz} \leqslant \nu \leqslant 1\,{\rm GHz}$ and to better than 1% for $\nu \gtrsim 1\,$GHz. We also checked the convergence for up to $n_{\rm max} = 180$ but with $n_{\rm split} = 2$ and reached to the same conclusion.

3.1.2 The influence of collisions

Here we wish to understand how the inclusion of collisions affects the hydrogen recombination spectrum. In Figure 4 we compare the results for the spectral distortions down to very low frequencies obtained for $n_{\rm max} = 100$ in three different calculations: case $\mathcal{A}$: $n_{\rm split} = 2$; case $\mathcal{B}$: $n_{\rm split} = n_{\rm max}$, no collisions; case $\mathcal{C}$: $n_{\rm split} = n_{\rm max}$, with collisions.

First one can clearly see the difference in the slope of the distortions in the range $0.1\,{\rm GHz} - 10\,{\rm GHz}$ for the cases $\mathcal{B}$ and $\mathcal{C}$ in comparison with case $\mathcal{A}$. At frequencies below $\nu \sim 2\,$GHz the solution for case $\mathcal{A}$ lies well above the other two solutions. The solution for case $\mathcal{B}$ cuts off at $\nu \sim 200\,$MHz, while the ones for the cases $\mathcal{A}$ and $\mathcal{C}$ reach down to $\nu \sim 45\,$MHz. This shows that *without collisions* transitions with $\Delta n \ll n$ at large n are disfavored and electrons reaching states $l \ll n$ to a large fraction depopulate via transitions with $\Delta n \sim n$, which increases the emission at higher frequencies (see also RMCS06). In addition one can conclude that for case $\mathcal{A}$ and $\mathcal{C}$ the cascade of electrons within the high l-states starts to become similarly important. However, since the populations of the very low shells ($n \leqslant 20-30$) are not significantly altered by collision, at low frequencies the distortions for case $\mathcal{C}$ cannot reach the same level as in the case $\mathcal{A}$, simply because the net radiative rates and population of the high shells critically depend on the cascade to lower shells.

We have checked, that increasing the rates for l-changing collisions by a large factor ($\sim 10^4 - 10^6$) we can recover the solution like for $n_{\rm split} = 2$. Furthermore we have performed additional calculations with $n_{\rm max} > 100$ and $n_{\rm split} = 100$ in order to check how this affects the recombination spectrum. We found that it only influences the distortions close to the lowest frequencies and still there the level of the case $\mathcal{A}$ is not reached. Therefore we conclude that the difference in the slopes of the recombination spectrum for case $\mathcal{A}$ and $\mathcal{C}$ at low frequencies will remain, even for $n_{\rm max} = n_{\rm split} > 100$.

We also studied how important in particular n-changing collisions are by performing computations only including l-changing collisions. In this case the spectrum practically remained unchanged (differences $\lesssim 1\%$ at the very low frequencies). In addition we ran computations artificially increasing the rate of n-changing collisions by a factor of 100. Here we found that the recombination emission at low frequencies was slightly reduced (at most by factor of ~ 2 for $\nu < 100\,$MHz in this case). This is due to the fact that in this case the net rate connecting two levels with large n includes a sizeable non-radiative contribution. One would expect that this, in addition to free-free absorption, may lead to a reduction of emission at very low frequencies, simply because n-changing collisions should dominate over radiative transitions for some large value of n, but it seems that this will only happen for $n_{\rm max} > 100$ and correspondingly at even lower frequencies than considered here.

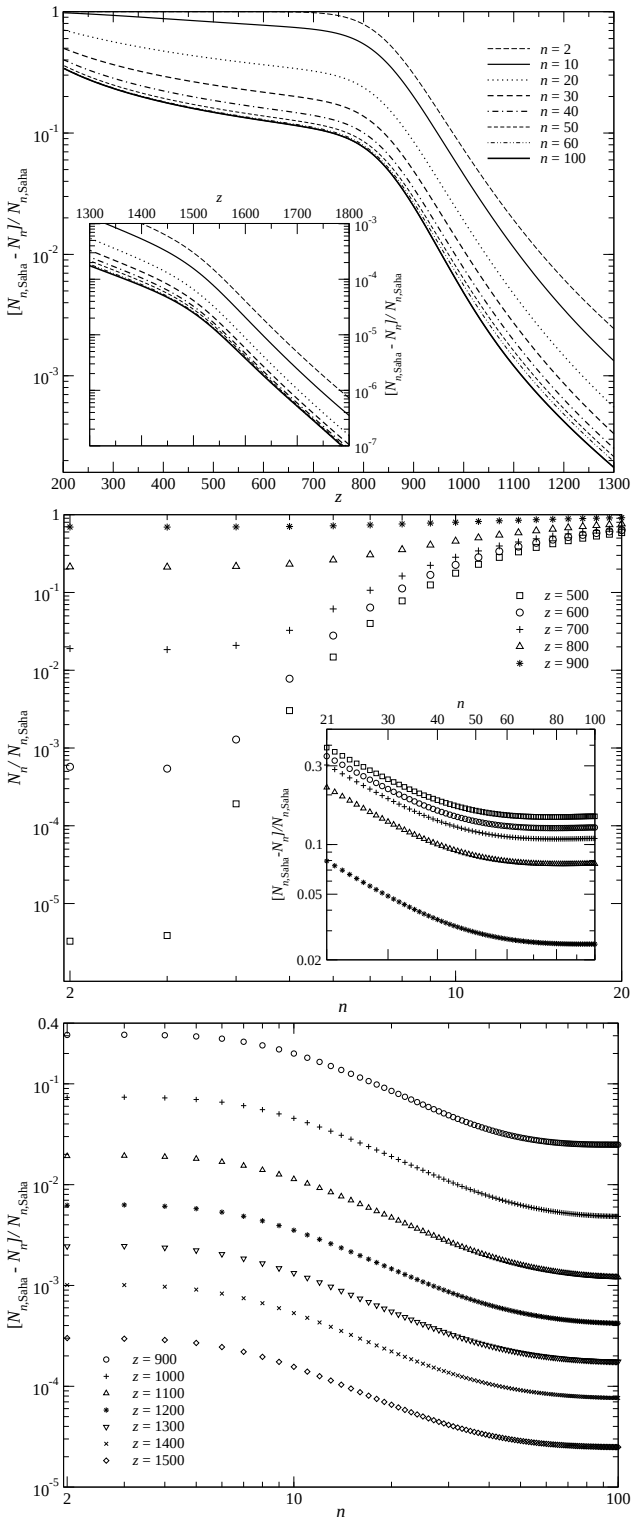

Figure 5. Departures of the total populations from Saha: N_n denotes the total population of shell n as obtain in our 100 shell computation with $n_{\rm max} = n_{\rm split}$ including collisions. $N_{n,{\rm Saha}}$ is the expected Saha-population relative to the continuum.

3.2 Populations of the levels

In this Section we discuss the structure of the hydrogen level populations in some more detail. At redshifts $z \leqslant 1500$ the ground state population always is extremely far from Saha-equilibrium with the free electrons. We therefore omitted it in the following.

Figure 5 shows the departures of the total populations for given n from the expected Saha population relative to the continuum. At high redshifts ($z \gtrsim 1800$), for all shells with $n \geqslant 2$ the departures from Saha are $\lesssim 10^{-7} - 10^{-6}$. At $z \sim 1500$ the departures reach a level of $\sim 10^{-5} - 10^{-4}$ and for $z \lesssim 1500$ all the curves become flatter, because from there on recombination is controlled by the escape of photons from the Lyman-α transition. At $z \sim 800$ the deviations from Saha exceed $\sim 10\%$ for all the considered shells and below that redshift they only change within a factor of $\sim 2 - 5$ until redshift $z = 200$. In general one can also see that for shells with $n \lesssim 10$ the departures from Saha are typically larger than for higher n and that below $z \sim 800$ the total populations of these levels are overestimated by many orders of magnitude when applying the Saha-relation with respect to the continuum. Note that during the whole epoch of recombination the total population of any shell is *smaller* than the expected Saha value.

In addition one can look at the deviations of the populations within a given shell from full statistical equilibrium (SE) over the l sub-levels. In Figures 6 and 7 we show the non-equilibrium effects on the populations of the angular momentum sub-states at different redshifts and given n for our computations with $n_{\rm max} = n_{\rm split} = 100$. In each panel the results obtained *with* and *without* the inclusion of l-changing and n-collisions are presented. In general one can state that departures from full SE become smaller the higher the redshift and the larger the value of n is. For $n = 30$ the inclusion of collisions does not alter the results significantly at *any* redshift, while for $n = 50$ one can see that within the high l-states the deviations from SE start to vanish. For $n = 80$ and $n = 100$ within the high l-states the deviations from full SE are very small down to redshifts $z \sim 1100-1200$ and even in the low l-states departures from SE start to be wiped out.

But still even for $n_{\rm max} = 100$ there is no shell beyond which full SE is reached for *all* the angular momentum sub-states. All the low l-states are underpopulated as compared to full SE. This is likely due to the fact that for $n \gtrsim 40$ these levels can all connect more or less directly with shells $n \lesssim 30$, which are always rather far from SE. Also the coupling to the continuum due to the l-scaling of the photoionization Gaunt factor is much stronger than for large l. Even for $n = 100$ the l-changing collisions are not able to significantly modify the low-l-populations set by the radiative rates. However, one still expects that increasing $n_{\rm max}$ for some $n > 100$ also the low l-states will reach full SE. Unfortunately due to computational constraints with $n_{\rm split} = n_{\rm max}$ we were not able to go beyond $n_{\rm max} \sim 100$. We conclude that for the cosmological hydrogen recombination calculations l-changing collisions become important for shells with $n \gtrsim 30 - 40$, as already estimated in RMCS06, but n-changing collisions may be neglected for shells with $n \lesssim 100$.

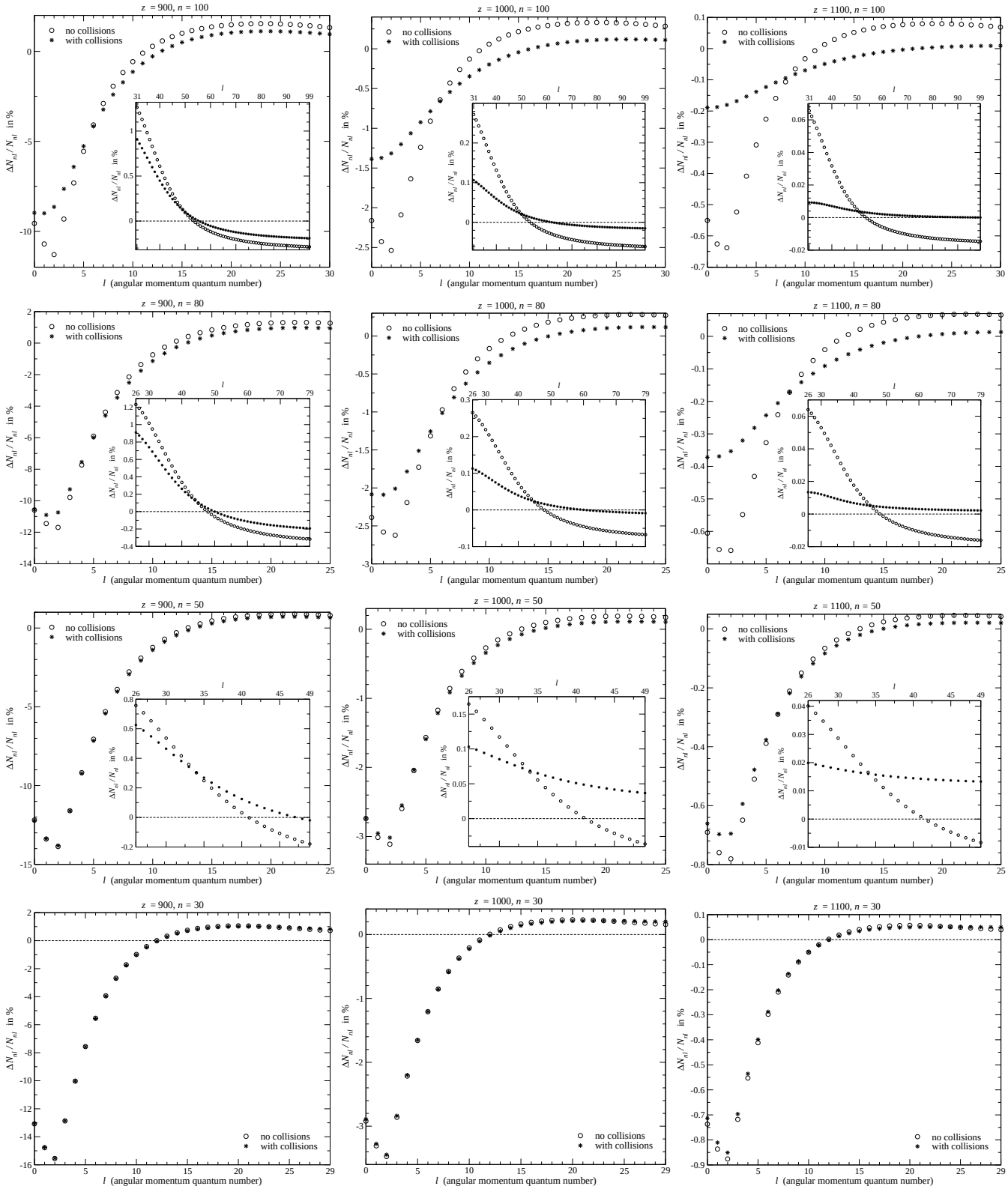

Figure 6. Non-equilibrium effects on the populations of the angular momentum sub-states for our computation with $n_{\rm max} = n_{\rm split} = 100$ at different redshifts and given n. The left column is for $z = 900$, the middle for $z = 1000$ and the right for $z = 1100$. The computations were performed for $n_{\rm max} = 100$ following the populations of all the angular momentum sub-states separately. In each panel the results obtained with and without the inclusion of l- and n-changing collisions are given. We present $\Delta N_{nl}/N_{nl} \equiv [N_{nl} - N_{nl}^{\rm SE}]/N_{nl}^{\rm SE}$, where the statistical equilibrium (SE) population is computed from the actual total population of the shell by $N_{nl}^{\rm SE} = [(2l+1)/n^2]N_{\rm tot}$.

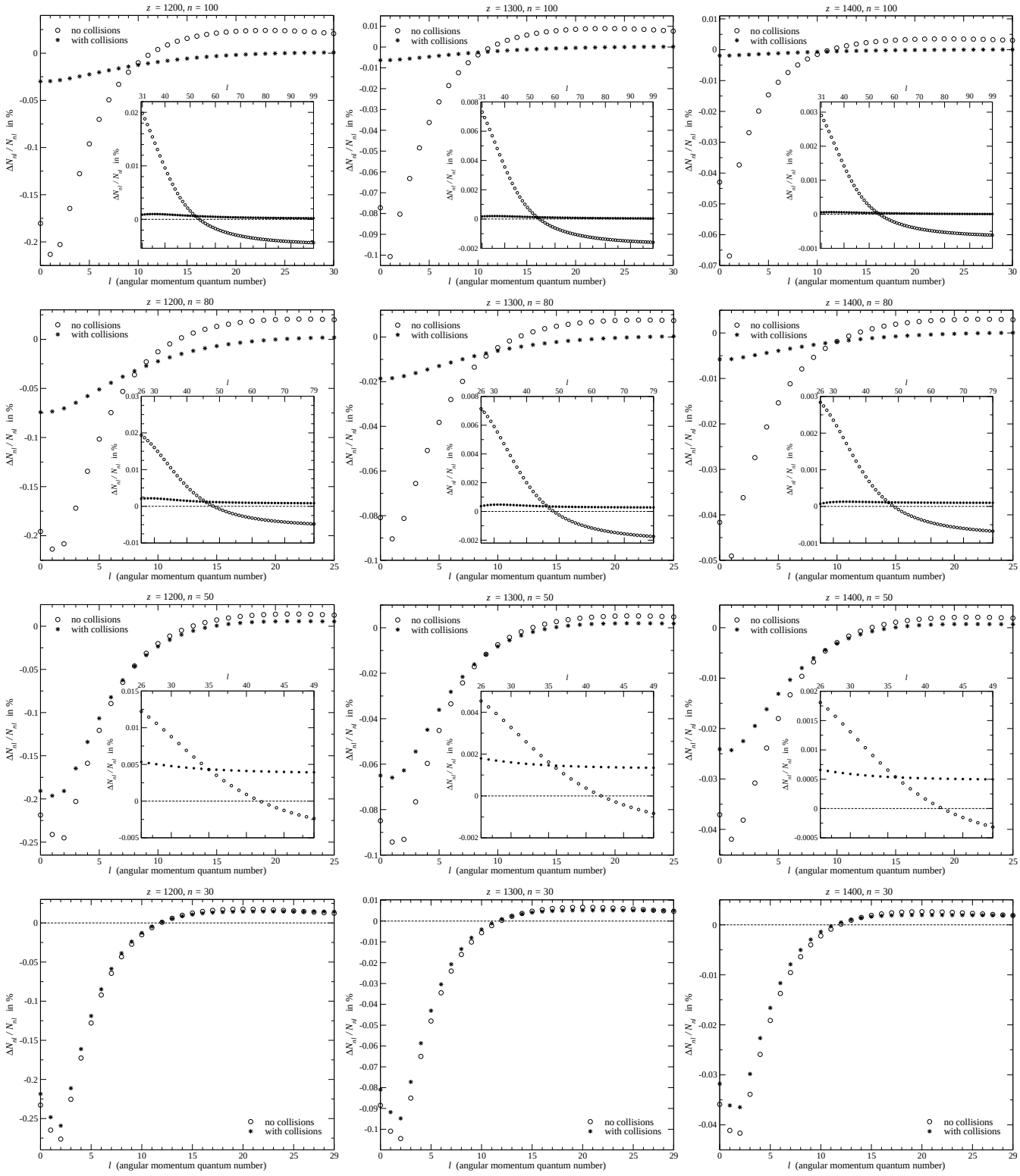

Figure 7. Non-equilibrium effects on the populations of the angular momentum sub-states for our computation with $n_{\rm max} = n_{\rm split} = 100$ at different redshifts and given n. The left column is for $z = 1200$, the middle for $z = 1300$ and the right for $z = 1400$. The computations were performed for $n_{\rm max} = 100$ following the populations of all the angular momentum sub-states separately. In each panel the results obtained with and without the inclusion of l- and n-changing collisions are given. We present $\Delta N_{nl}/N_{nl} \equiv [N_{nl} - N_{nl}^{\rm SE}]/N_{nl}^{\rm SE}$, where the statistical equilibrium (SE) population is computed from the actual total population of the shell by $N_{nl}^{\rm SE} = [(2l+1)/n^2]N_{\rm tot}$.

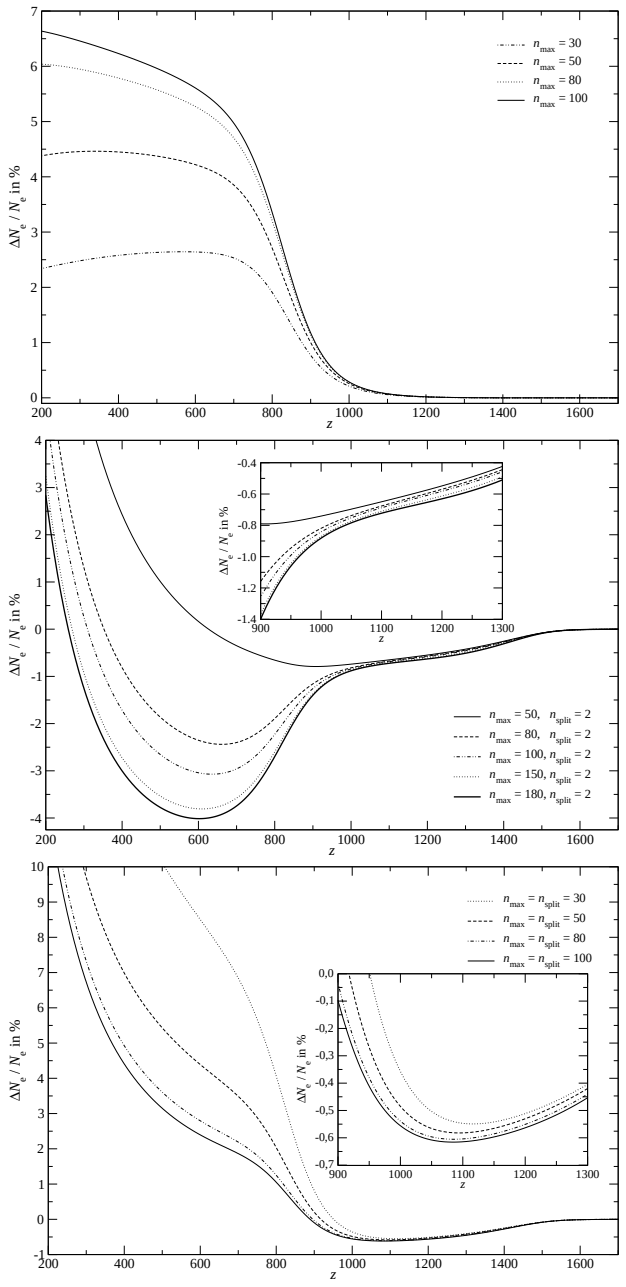

Figure 8. Relative difference in the free electron fraction, $\Delta N_{\rm e}/N_{\rm e}$, for different values of $n_{\rm max}$. The upper panel shows the comparison for our computations with $n_{\rm split} = n_{\rm max}$ with the results for $n_{\rm split} = 2$. In the middle panel we compare our computations for $n_{\rm split} = 2$ with the output of RECFAST and in the lower panel we show the relative difference for our computations with $n_{\rm split} = n_{\rm max}$ with respect to the RECFAST output.

3.3 Effects on the free electron fraction and comparison with RECFAST

In the upper panel of Fig. 8 we show the relative difference in the free electron fraction for our computations with $n_{\rm split} = n_{\rm max}$ as compared to the results for $n_{\rm split} = 2$. At low redshifts this difference exceeds the level of 5%, showing that when following the populations of all the angular momentum sub-states separately recombination is slightly slower. However, it seems that close to the maximum of the Thomson visibility function ($z_{\rm dec} \sim 1090$ and $\Delta z \sim 195$) departures from full SE within the shells are not sufficiently large to modify the recombination history. At $z \sim 500$ the relative difference for the case $n_{\rm max} = 100$ is more than 2 times bigger than for $n_{\rm max} = 30$. Also in the redshift range $z \gtrsim 700$ the ratio of these two curves remains greater than ~ 1.2. Including more than 100 shells into the calculation seems necessary in order to reach full convergence at all redshifts.

In the middle panel of Fig. 8 we present the direct comparison of our results with the output of RECFAST[4] for different cases with $n_{\rm split} = 2$ up to $n_{\rm max} = 180$. During the peak of the visibility function the difference is close to -0.7% and only reaches $\sim 1\%$ and $\sim 3\%$ for $z \sim 960$ and $z \sim 780$, respectively. This comparison shows that representing the full multi-level calculation with percent-level accuracy in the full range of redshifts probably requires some more general 'fudge-function' instead of a single 'fudge-factor'. Also, the difference at $z \gtrsim 1000$ is probably not related to the detailed treatment of the populations in the angular momentum sub-states but points towards the limitations of the effective 3-level approach. A detailed analysis will be left for some future work.

Finally, in the lower panel of Fig. 8 we show the direct comparison of our results for different calculations with $n_{\rm max} = n_{\rm split}$ with the output of RECFAST. There is a difference of roughly -0.6% in the electron fraction close to the peak of the visibility function. The results also suggest that at low redshifts recombination proceeds slightly slower than in the RECFAST code and that one can still expect more than a few percent corrections due to the detailed treatment of the populations in the angular momentum sub-states. However, one still has to push to a larger number of shells and very likely include more physics, such as details of helium recombination, collisional ionization and three-body recombination, collisional transitions with $|\Delta l| > 1$ or forbidden transitions. At low redshifts ($z \lesssim 300$), also details of the hydrogen chemistry may have to be reconsidered. In addition one should include a simultaneous treatment of other processes such as discussed by Dubrovich & Grachev (2005); Chluba & Sunyaev (2006b); Kholupenko & Ivanchik (2006); Novosyadlyj (2006) and likely more. Here especially the treatment of two-photon transitions for higher shells including stimulated emission or possibly other forbidden transitions may still lead to percent level differences in both the hydrogen recombination spectrum and the ionization history.

As an example, the strongest distortions of the CMB spectrum arising from the epoch of hydrogen recombination are due to the Lyman-α transition and the 2s two-photon decay. Previously, the feedback of these excess photons onto the photoionization rates for the second shell ($n = 2$) has been considered by Seager et al. (2000), yielding no significant changes in the ionization history. However, recently it has been shown by Kholupenko & Ivanchik (2006) that this huge excess of photons in the Wien-tail of the CMB leads to an increase of the 1s $\rightarrow$ 2s two-photon absorption rate,

[4] In fact we used our own implementation of this code, which solves the system of differential equations as given in (Seager et al. 1999) with accuracy better than 0.1%.

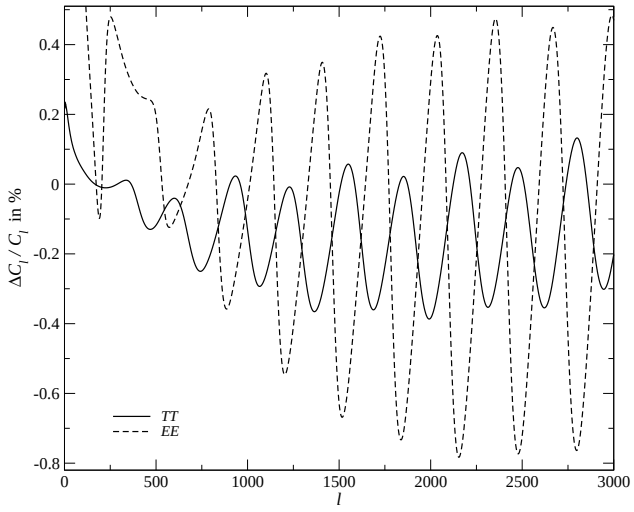

Figure 9. changes of the CMB temperature (TT) and polarization (EE) power spectra for our full computation with $n_{\rm max} = n_{\rm split} = 100$ including collisions.

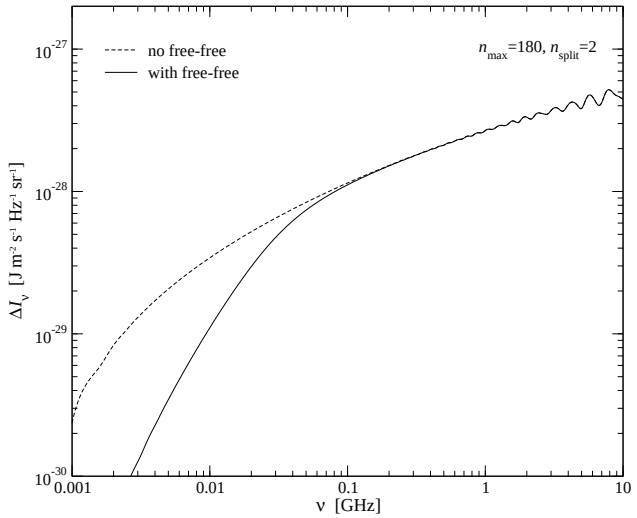

Figure 10. Effect of free-free absorption on the hydrogen bound-bound emission spectrum for $n_{\rm max} = 180$ and $n_{\rm split} = 2$. The spectrum in the range $\nu \gtrsim 100\,$MHz is not affected by the free-free process, whereas at $\nu \lesssim 1\,$MHz all the distortions are erased.

which results in percent-level corrections to the ionization history during hydrogen recombination. This feedback cancels a large part of the effect of induced two-photon decay of the 2s level as discussed by Chluba & Sunyaev (2006b) which again shows that reaching percent-level accuracy for recombination is not very simple.

We would like to point out that the simplification in connection with the computation of the photoionization and recombination rates, as described in Sect. 2.2, at low redshifts may still affect the results presented in Fig. 8 on the percent-level.

3.4 Changes in the CMB temperature and polarization power spectra

In order to compute the changes of the CMB temperature and polarization power spectra due to the differences in the ionization history we modified the RECFAST routine inside the latest version of CMBEASY (Doran 2005). Since we obtained the ionization history only in the redshift range $200 \leqslant z \leqslant 2100$ we had to *merge* the solution of RECFAST with our solution. At $z = 2100$ this was not problematic since there both solutions practically coincide. At $z \leqslant 200$ we simply rescaled the RECFAST output by a constant factor, such that the merged solution became continuous. We checked how this approach influences the obtained difference in the power spectra by changing the transitions redshift to $z = 300$. However, this only affected the changes in the power spectra at $l \lesssim 50 - 100$ on the level of percent and we expect that the results for $l \gtrsim 100 - 200$ are robust. Note that here l corresponds to the index of the spherical harmonic function Y_{lm} rather than the angular momentum quantum number for a level inside the hydrogen atom.

In Fig. 9 we give the difference in the temperature and polarization power spectra for our full computation with $n_{\rm max} = n_{\rm split} = 100$. The difference reaches the level of 0.4% for the TT and 0.8% for the EE power spectrum. We checked the convergence by using the results for different $n_{\rm max} < 100$ and found that the curves still changed at the percent-level when going from $n_{\rm max} = 80$ to 100. This shows that still more shells should be included and computations have to be extended down to $z = 0$ in order to obtain a definite answer.

4 ADDITIONAL PHYSICAL PROCESSES

4.1 Effects of free-free absorption

The free-free process is increasingly important at low frequencies and should eventually be able to wipe out any spectral distortion below some frequency $\nu_{\rm ff}$. Given the solutions for the recombination history and the emission resulting from each bound-bound transition one can also take the free-free process into account. Since at redshifts $z \gtrsim 1200$ the difference in the electron and photon temperature is very small, for simplicity we assumed $T_{\rm e} = T_\gamma = T_0(1+z)$ with todays CMB temperature $T_0 = 2.725\,$K. In Figure 10 we illustrate the effect of free-free absorption on the hydrogen recombination spectrum for $n_{\rm max} = 180$ and $n_{\rm split} = 2$. We chose this particular example, since we could obtain the distortions down to sufficiently low frequencies. Our calculations show that the recombination spectrum in the frequency range $\nu \gtrsim 100\,$MHz is not affected by the free-free process. However, for He III and probably He II recombination the effect of free-free absorption will be stronger, since the temperature and density of the plasma is larger and there are more electrons per helium atom when hydrogen is still fully ionized.

4.2 Effects of electron scattering

To estimate the effects of electron scattering one can calculate the expected broadening of an initially narrow line for a given recombinations history. Following Pozdniakov et al. (1979) for large Thomson optical depth $\tau = \int N_{\rm e}\sigma_{\rm T}\,{\rm d}l \gg 1$ and small Compton y-parameter $y = \int \frac{kT_{\rm e}}{m_{\rm e}c^2}\,{\rm d}\tau \ll 1$ the broadening due to electron scattering is dominated by the

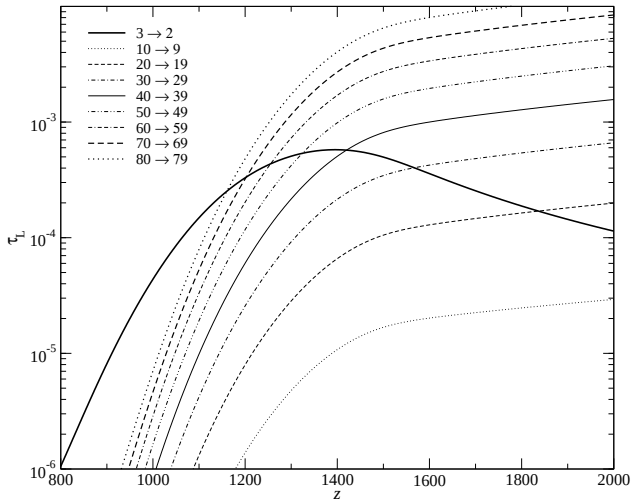

Figure 11. Line optical depth for some α-transitions within high shells. The results were obtained using the computations for 100 shells. For comparison the H_α-line ($3 \rightarrow 2$) optical depth is given.

Doppler effect and one can find: $\frac{\Delta\nu}{\nu}\big|_{\rm sc} \sim 2\sqrt{y\,\ln 2}$. Using the standard ionization history as obtained with the RECFAST code one finds that for the spectral distortions due to hydrogen recombination the broadening is less than percent for emission occurring at redshift $z \lesssim 1500$. Since the feature we are considering here are typically much broader ($\gtrsim 20\%$) one may neglected the effect of electron scattering on the hydrogen recombination spectrum. However, for He II and in particular for He III recombination this may not be true anymore due to two reason: first He III recombines at higher redshift ($z \sim 6000-6500$) than hydrogen ($z \sim 1100-1500$) and second because it occurred more rapidly. We shall not discuss these points any further here.

4.3 Imprint of the recombinational line transitions on the CMB angular power spectrum

Our detailed study of the hydrogen recombination permits us to evaluate the effects discussed on Rubiño-Martín et al. (2005), but now for shells above $n = 10$. In that paper, these authors discussed the imprint of the recombinational lines on the angular power spectrum of the CMB, via resonant scattering in the lines (see also Basu et al. 2004; Hernández-Monteagudo & Sunyaev 2005, for more details). Due to correlations with the existing radiation field, the net effect on the angular power spectrum, δC_ℓ, is proportional to the optical depth in the line, $\tau_{\rm L}$ (see Eq. 1 in Rubiño-Martín et al. 2005), at the relevant redshift. As shown in Rubiño-Martín et al. (2005), in the optically thin limit the first order correction to the visibility function has two terms. The first one is connected with *suppression* of existing anisotropies, and it is proportional to $\tau_{\rm L} \times \mathcal{V}_{\rm T}$, where $\mathcal{V}_{\rm T}$ is the Thomson visibility function (Sunyaev & Zeldovich 1970). The second term is associated to *generation* of new anisotropies, and it is proportional to $\tau_{\rm L} \times \exp(-\tau_{\rm T})$. Note that here l corresponds to the index of the spherical harmonic function Y_{lm} rather than the angular momentum quantum number for a level inside the hydrogen atom.

Since the bound-bound recombination lines are very narrow as compared to the duration of recombination, fixing the observing frequency one tunes to the signal arising during one particular epoch of recombination. Under the assumption that the maximal signal for all the bound-bound recombination lines arises at the same redshift this implies that going to lower frequencies the effect is dominated by the signal coming from the α-transitions of higher shells.

In Fig. 11 we present the optical depth to resonant scattering for several main transitions ($\Delta n = 1$) between high shells of the hydrogen atom and we compare these to the one corresponding to H_α. Although the optical depths for $n \gtrsim 20$ exceed the one for H_α at high redshifts, the expected signature in the power spectrum will be small due to the presence of Thomson scattering. However, this process might become interesting in the future because at low frequencies the signals of many transitions overlaps and one expects that for a given bandwidth of the experiment a superposition of the contributions with comparable amplitude might amplify the signal. This may increase the total change in the temperature power spectrum notably, especially at frequencies below $\sim 1\,$GHz. We have computed the effect on the power spectrum and found that for $\nu \sim 50-100\,$MHz it is comparable to the signal produced by the scattering within the H_α-transition. Our computations also showed that a similar process due to the *absorption* and *re-emission* of photons in the continuum also leads to weak fluctuations on the level of $\delta C_\ell \ell(\ell+1)/2\pi \approx 9\times10^{-4}\mu{\rm K}^2$ at 1.4 GHz. This signal also shows a characteristic oscillatory behaviour, and again it is maximum at small angular scales ($\ell \sim 900$).

5 CONCLUSION

We presented results for the spectral distortions of the CMB arising during the epoch of cosmological hydrogen recombination due to bound-bound transition with observing frequencies down to $\nu \sim 100\,$MHz and confirm that the relative spectral distortions, $\Delta I_\nu/B_\nu$, are rapidly growing towards low frequencies. We show that even within the highest considered shell full statistical equilibrium is not reached and that at low frequencies the recombination spectrum is significantly different when full SE for shells with $n > 2$ is assumed. We also conclude that in cosmological hydrogen recombination calculations l-changing collisions should be included for shells with $n \gtrsim 30-40$, but n-changing collisions can be neglected for shells with $n \lesssim 100$.

In Sect. 3.3 we have presented our results for the ionization fraction as compared to the RECFAST output. Including a treatment of the populations of all the individual angular momentum sub-states slows recombination down, leaving a $\gtrsim 5-10\%$ larger residual electron fraction at low redshifts. Although the overall effect on the temperature and polarization power spectra due to the changes in the recombination history is $\lesssim 1\%$ these additional electrons may be important in computations of the first stars and structures (Barkana & Loeb 2001; Bromm et al. 2002), for which especially the formation of molecular hydrogen plays a crucial role. The discussion has shown that representing the full multi-level calculation with percent level accuracy in the full range of redshifts probably requires some more general 'fudge-function' instead of a single 'fudge-factor'. Also, one still has to push to a larger number of shells and very

likely include more physics. For extensive calculations of the CMB temperature and polarization power spectra it will become important to develop a new simplified and fast scheme which accurately models the physics during the recombination epoch.

ACKNOWLEDGMENTS

We thank Moncef Derouich for useful discussions about collisional rates. We also acknowledge use of CMBEASY (Doran 2005). In addition J.C. and R.S would like to thank the Institute for Theory and Computation of the Harvard University and the Institute of Advanced Study, Princeton, for their hospitality during a visit in Sept. 2006 and useful conversations at the final stages of this paper.

REFERENCES

Barkana R., Loeb A., 2001, Physics Reports, 349, 125
Basu K., Hernández-Monteagudo C., Sunyaev R. A., 2004, A&A, 416, 447
Beigman I. L., Sunyaev R. A., 1978, preprint Leb. Phys. Inst. N163
Brocklehurst M., 1971, MNRAS, 153, 471
Bromm V., Coppi P. S., Larson R. B., 2002, ApJ, 564, 23
Chluba J., Sunyaev R. A., 2006a, astro-ph/0608120
Chluba J., Sunyaev R. A., 2006b, A&A, 446, 39
Doran M., 2005, Journal of Cosmology and Astro-Particle Physics, 10, 11
Dubrovich V. K., 1975, Soviet Astronomy Letters, 1, 196
Dubrovich V. K., Grachev S. I., 2005, Astronomy Letters, 31, 359
Dubrovich V. K., Shakhvorostova N. N., 2004, Astronomy Letters, 30, 509
Dubrovich V. K., Stolyarov V. A., 1995, A&A, 302, 635
Hernández-Monteagudo C., Sunyaev R. A., 2005, MNRAS, 359, 597
Hinshaw G., Nolta M. R., Bennett C. L., Bean R., Dore' O., Greason M. R., Halpern M., Hill R. S., Jarosik N., Kogut A., Komatsu E., Limon M., Odegard N., Meyer S. S., Page L., Peiris H. V., Spergel D. N., Tucker G. S., Verde L., Weiland J. L., 2006, ArXiv Astrophysics e-prints
Hummer D. G., Storey P. J., 1987, MNRAS, 224, 801
Karzas W. J., Latter R., 1961, ApJS, 6, 167
Kholupenko E. E., Ivanchik A. V., 2006, Astronomy Letters, in press
Kholupenko E. E., Ivanchik A. V., Varshalovich D. A., 2005, Gravitation and Cosmology, 11, 161
Lewis A., Weller J., Battye R., 2006, astro-ph/0606552
Liubarskii I. E., Sunyaev R. A., 1983, A&A, 123, 171
Novosyadlyj B., 2006, MNRAS, 370, 1771
Page L., Hinshaw G., Komatsu E., Nolta M. R., Spergel D. N., Bennett C. L., Barnes C., Bean R., Dore' O., Halpern M., Hill R. S., Jarosik N., Kogut A., Limon M., Meyer S. S., Odegard N., Peiris H. V., Tucker G. S., Verde L., Weiland J. L., 2006, ArXiv Astrophysics e-prints
Peebles P. J. E., 1968, ApJ, 153, 1
Pengelly R. M., Seaton M. J., 1964, MNRAS, 127, 165
Pozdniakov L. A., Sobol I. M., Sunyaev R. A., 1979, A&A, 75, 214
Rubiño-Martín J. A., Chluba J., Sunyaev R. A., 2006, MNRAS, 371, 1939
Rubiño-Martín J. A., Hernández-Monteagudo C., Sunyaev R. A., 2005, A&A, 438, 461
Rybicki G. B., dell'Antonio I. P., 1993, in Chincarini G. L., Iovino A., Maccacaro T., Maccagni D., eds, ASP Conf. Ser. 51: Observational Cosmology Spectral Distortions in the CMB from Recombination.. pp 548–+
Seager S., Sasselov D. D., Scott D., 1999, ApJL, 523, L1
Seager S., Sasselov D. D., Scott D., 2000, ApJS, 128, 407
Storey P. J., Hummer D. G., 1991, Computer Physics Communications, 66, 129
Sunyaev R. A., Zeldovich Y. B., 1970, Astrophysics and Space Science, 7, 3
van Regemorter H., 1962, ApJ, 136, 906
Wong W. Y., Seager S., Scott D., 2006, MNRAS, 367, 1666
Zeldovich Y. B., Kurt V. G., Syunyaev R. A., 1968, Zhurnal Eksperimental noi i Teoreticheskoi Fiziki, 55, 278